Molecular Therapy
Original Article

Combination of *In Situ Lcn2* pRNA-RNAi Nanotherapeutics and iNSC Transplantation Ameliorates Experimental SCI in Mice

Alice Braga,[1] Sara Bandiera,[1] Jeroen Verheyen,[1] Regan Hamel,[1] Carola Rutigliani,[1] Frank Edenhofer,[2] Jayden Aaron Smith,[1,3] and Stefano Pluchino[1]

[1]Department of Clinical Neurosciences and NIHR Biomedical Research Centre, University of Cambridge, CB2 0HA Cambridge, UK; [2]Department of Molecular Biology & CMBI, Genomics, Stem Cell Biology & Regenerative Medicine, Leopold-Franzens-University Innsbruck, 6020 Innsbruck, Austria; [3]Cambridge Innovation Technologies Consulting, Ltd., CB4 0WS Cambridge, UK

Spinal cord injury (SCI) is a debilitating neurological condition characterized by different cellular and molecular mechanisms that interplay in exacerbating the progression of the pathology. No fully restorative therapies are yet available, and it is thus becoming recognized that combinatorial approaches aimed at addressing different aspects of SCI will likely results in greater functional outcomes. Here we employed packaging RNA-mediated RNA interference (pRNA-RNAi) nanotherapeutics to downregulate *in situ* the expression of *lipocalin 2* (*Lcn2*), a known mediator of neuroinflammation and autocrine mediator of reactive astrogliosis, and to create a more amenable niche for the subsequent transplantation of induced neural stem cells (iNSCs). To our knowledge, this is the first approach that takes advantage of the modular and multifunctional pRNA three-way junction platform in the SCI niche, while also exploiting the therapeutic potential of immune-compatible and feasible iNSC transplants. We show the combination of such treatments in a mouse model of contusion thoracic SCI leads to significant improvement of locomotor function, albeit not better than single pRNA-RNAi treatment, and results in synergistic histopathological effects, such as reduction of glial scar volume, diminished pro-inflammatory response, and promotion of neuronal survival. Our results provide evidence for a novel combinatorial approach for treating SCI.

INTRODUCTION

Spinal cord injury (SCI) is a devastating neurological disorder that affects thousands of individuals each year.[1] Traumatic injuries (i.e., caused by trauma or damage resulting from the application of an external force of any magnitude, such as in the event of road traffic crashes or falls) have a higher rate of incidence compared to non-traumatic injuries (i.e., congenital/genetic malformations, damage caused by infection, loss of blood supply, or slow degeneration of the vertebrae).[2] Despite the great progress made in recent decades in understanding the molecular and cellular events initiated by traumatic SCI, fully restorative treatments are not yet available.[3] SCI is characterized by a primary injury that develops into a variety of secondary molecular and cellular events, including glial scarring, astrogliosis, the activation and recruitment of an inflammatory response, and ongoing cell death.[4] Due to this multifaceted nature, it is becoming increasingly clear that combination approaches aimed at targeting different aspects of the pathology will likely result in a more successful translation to human therapies.[5]

Among the most attractive experimental therapeutic approaches, stem cell transplantation has emerged as a promising tool, aiming at cellular replacement and modulating the injured environment by means of a series of striking chaperone effects.[6,7] Transplanted neural stem cells (NSCs) are capable of establishing a crosstalk with an injured or inflammatory host environment, wherein they promote tissue protection through mechanisms including the release of immunomodulatory molecules or trophic growth factors,[8] or by sequestration of pro-inflammatory metabolites.[9] While NSCs have elicited promising results, the last few decades have seen the development of novel technologies for the generation of induced-pluripotent stem cells (iPSCs), leading to the possibility of an easily accessible cell source and the possibility of autologous transplantation.[10] The induced NSCs (iNSCs) employed in this study represent an even more promising technology, with the direct reprogramming of autologous somatic cells into stably expandable NSCs being fast and involving less manipulation compared to iPSC technology,[11,12] and therefore less chance to develop adverse effects *in vivo* (i.e., teratomas) after cellular grafting.[13]

Lipocalin 2 (Lcn2), a 25 kDa protein belonging to the lipocalin family, is a crucial player in multiple biological functions, notably as an

Received 16 April 2020; accepted 2 August 2020;
https://doi.org/10.1016/j.ymthe.2020.08.001.

Correspondence: Jayden Aaron Smith, Cambridge Innovation Technologies Consulting Ltd., CB4 0WS Cambridge, UK.
E-mail: jayden.smith@citc-ltd.co.uk
Correspondence: Stefano Pluchino, Department of Clinical Neurosciences and NIHR Biomedical Research Centre, University of Cambridge, CB2 0HA Cambridge, UK.
E-mail: spp24@cam.ac.uk

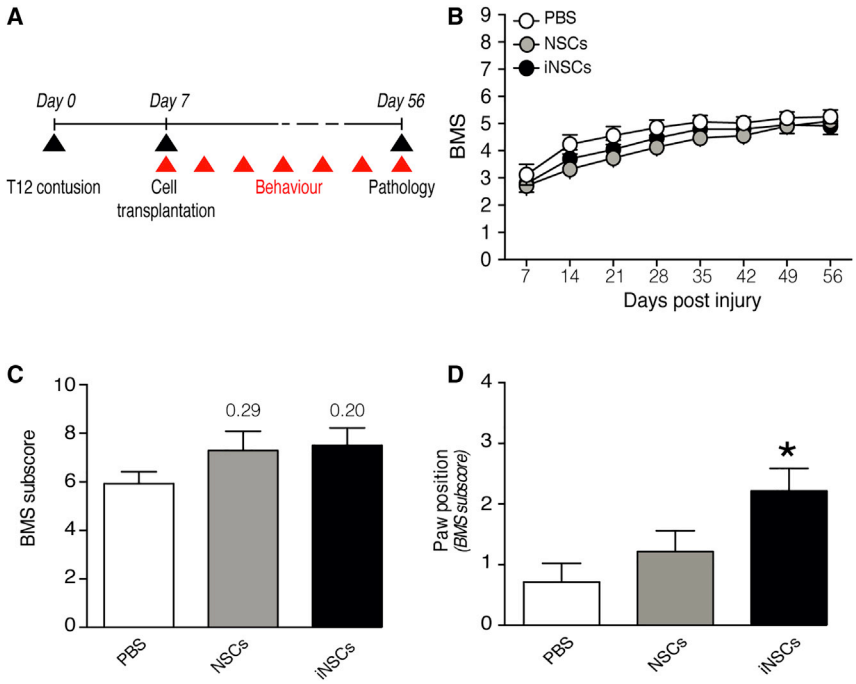

Figure 1. The Subacute Transplantation of NSCs or iNSCs Promotes Recovery of Fine Locomotor Capabilities

(A) Experimental design for the subacute transplantation of fGFP-NSCs or fGFP-iNSCs and behavioral assessments. *Ex vivo* pathology is performed at 56 dpi. (B) Basso Mouse Scale (BMS) score evaluation of motor function recovery. Data are mean values (±SEM) from n ≥ 13 mice per group. (C) Evaluation of fine movement capabilities through BMS sub-score, and (D) the specific paw position sub-score parameter at 56 dpi. Data are mean values (±SEM) from n ≥7 mice per group. *p < 0.05, versus PBS. dpi, days post injury.

immunomodulatory agent, and therefore its dysregulation has been revealed to be a key factor in many pathologies.[14] Within the central nervous system (CNS), various cell types upregulate Lcn2 in a disease context, including activated microglia,[15] infiltrating neutrophils,[16] and reactive astrocytes.[17] Of particular interest is the study from Rathore et al.;[18] the authors observed a significantly lower inflammatory response and reduced secondary damage in *Lcn2*-knockout (KO) mice subjected to SCI. We thus sought to employ RNA nanotechnology in order to modulate *Lcn2* expression.

RNA-based nanostructures offer several advantages compared to other nanocarriers, possessing intrinsically defined features at the nanometer scale, being characterized by relatively high thermal stability and structural flexibility, and moreover the capability to perform a variety of different functions, such as RNA interference (RNAi).[19] A promising example of this technology, specific to the purposes of this study, are the bio-inspired packaging RNA (pRNA)-RNAi nanostructures. The constructs' advantageous size, thermodynamic stability, resistance to chemical denaturation, and modular nature make them suitable candidates for translational approaches.[20] pRNA-RNAi nanostructures are connected by a highly stable three-way junction (3WJ) region that can be manipulated and derivatized in order to obtain multi-armed, multi-functional structures. This platform has previously shown great potential, primarily in cancer-therapeutic approaches,[21] without cytotoxicity or immunogenicity.[22]

Moreover, we previously showed that 3WJs bearing small interfering RNA (siRNA) against *Lcn2* efficiently downregulated the target gene in an *in vitro* culture system of resting and activated astrocytes, and preliminary *in vivo* experiments showed a significant downregulation of *Lcn2* after delivery of an anti-*Lcn2* 3WJ (3WJ-L12) in a model of contusive SCI.[23]

In our study, we aimed at combining these two innovative approaches: the *in situ* injection of pRNA-RNAi nanoparticles targeting *Lcn2*—herein employed *in vivo* for the first time within a non-cancer CNS-disease context—and the transplantation of murine-derived iNSCs in a rodent model of moderate contusive thoracic SCI. We evaluated the synergistic therapeutic potential of this approach, assessing outcomes with regard to functional recovery and the effects on secondary mechanisms arising from SCI.

RESULTS

NSC and iNSC Grafts Ameliorate Moderate Contusive Thoracic SCI in Mice

We first tested the therapeutic potential of subacute (7 days post injury, dpi) focal transplantation of murine-derived farnesylated GFP (fGFP)-iNSCs into the spinal cord of mice subjected to moderate (70 kdyne) contusive SCI. In order to investigate the capability of iNSCs to promote functional recovery upon transplantation, we compared them to the well-characterized bona fide fGFP-NSCs derived from adult mice[24,25] transplanted in the same animal model (Figure 1A). Up to 49 days post-transplantation (dpt) we did not observe any significant differences in locomotor functions between transplanted groups and the control (phosphate buffered saline [PBS]-vehicle-only) group (Figure 1B). Nevertheless, moderate SCI in mice has been shown to lead to spontaneous recovery over time[26] that might hamper any observation of beneficial aspects of the treatments. Moreover, the Basso Mouse Scale (BMS) represents an overall score, unable to discriminate between specific aspects of locomotion like paw position, coordination, stepping frequency, trunk stability, and tail position. For these reasons, we investigated the total BMS sub-score in each of the three groups at 56 dpi (49 dpt), observing a moderate increase in both iNSC and NSC groups (Figure 1C).

We then investigated the individual locomotor features comprising the BMS sub-score among the three groups, revealing a significant

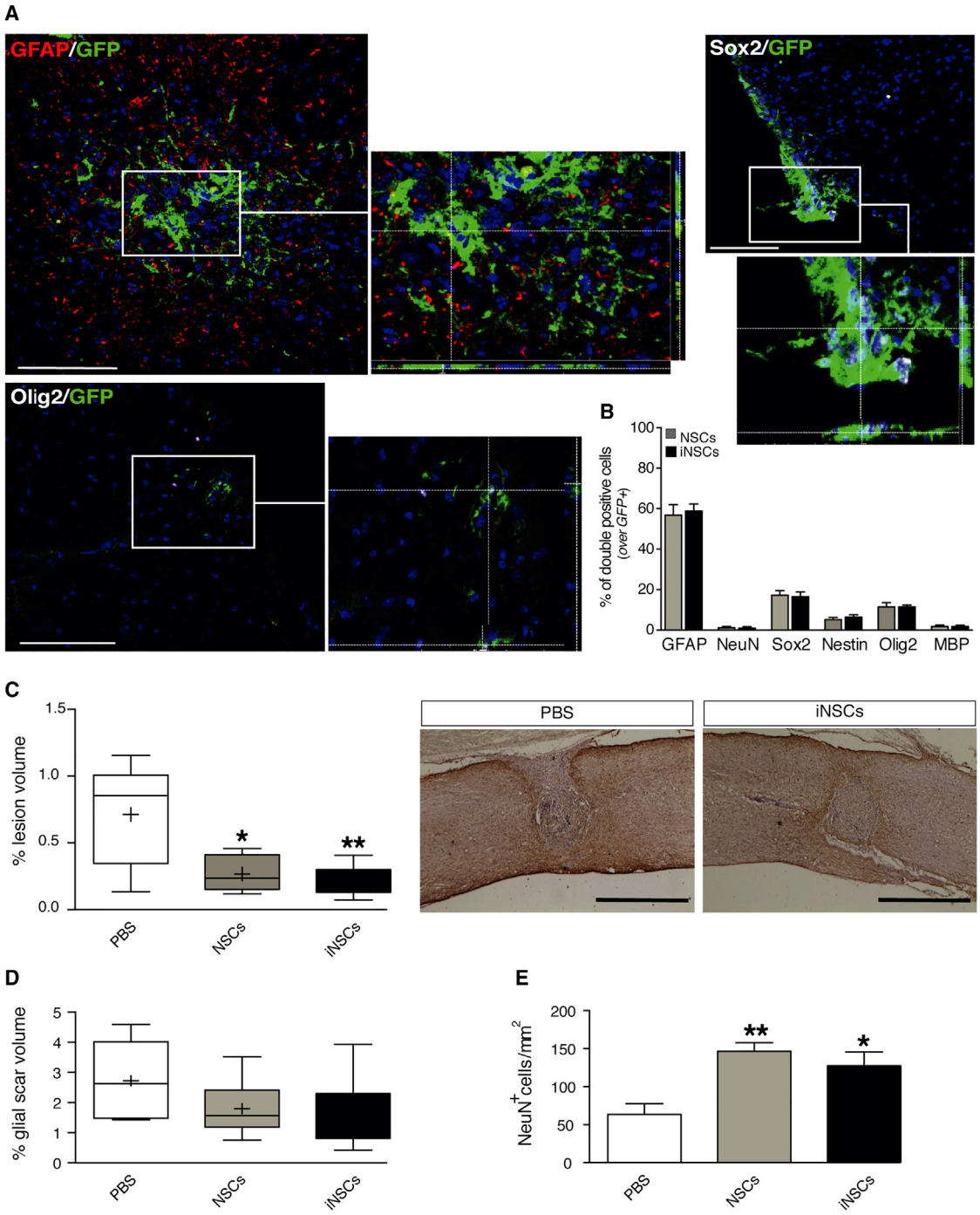

Figure 2. The Subacute Transplantation of NSCs or iNSCs Promotes Tissue Healing and Neuronal Survival

(A) Representative immunofluorescence micrographs depicting engrafted fGFP-iNSCs, co-expressing the astroglial marker GFAP (red), the stem cell marker Sox2 (white), or the immature oligodendroglial marker Olig2 (white) at 56 dpi. White rectangular area points to magnification snapshots with z stack. (B) Quantification of engrafted GFP-positive cells co-expressing differentiation markers following transplantation into the injured spinal cord at 56 dpi. Data are as mean % of double-positive cells over the total number of GFP-positive cells (±SEM), from n = 3 mice per group. (C) Stereological quantification of lesion volumes expressed as % of lesion volume over the volume of selected spinal cord segment. Data represent minimum to maximum volume from n ≥ 5 mice per group. Representative bright-field images (right) from control (PBS) and fGFP-iNSC groups. GFAP is in brown and cell nuclei are counterstained with hematoxylin. *$p < 0.05$ and **$p < 0.01$, versus PBS. (D) Stereological quantification of glial scar

(legend continued on next page)

improvement in paw position for the iNSC group (Figure 1D) and a significantly improved coordination for the NSC group (Figure S1A). We did not observe differences between treatment groups for the remaining parameters (Figure S1A).

In order to evaluate the possibility of the development of hindlimb allodynia upon transplantation, defined as an increased sensitivity to noxious stimuli,[27] the von Frey hair test and Hargreaves test were performed on the three groups. Transplantation of either fGFP-NSCs or fGFP-iNSCs did not show any significant decrease in the threshold of response to mechanical allodynia, nor did we observe any induction in pain sensitivity (Figure S1B).

Thus, *in vivo* evaluation of iNSCs revealed a similar capability to that of bona fide NSCs in promoting fine locomotor functions.

Engrafted iNSCs Differentiate and Promote Tissue Healing in the Injured Spinal Cord

We then sought to characterize engrafted fGFP-iNSCs upon transplantation into the host tissue and assess the effects of transplantation on major secondary events involved in SCIs, including aspects such as lesion volume and glial scarring. All histological analyses were conducted at 56 dpi (49 dpt).

We found that fGFP-iNSC and fGFP-NSC transplants displayed a similar percentage of surviving engrafted cells over the total number of transplanted cells, 5.9% ± 0.85% and 6.9% ± 1.6%, respectively (Figure S2A). Cells were transplanted in four different sites surrounding the lesion area within the spinal cord parenchyma, approximately 500 μm distant from the lesion site, and by 7 weeks post-transplantation both fGFP-iNSCs and fGFP-NSCs were found accumulated toward the lesion epicenter to a similar extent (Figure S2B).

Engrafted cells were then phenotypically evaluated. We observed that the majority of fGFP-iNSCs and fGFP-NSCs expressed the astroglial lineage marker glial fibrillary acidic protein (GFAP) (59% ± 3.4% and 57% ± 5.3%, respectively) (Figures 2A and 2B). A very small proportion of grafted iNSCs were found differentiated toward a neuronal nuclei (NeuN)-positive neuronal lineage marker (0.93% ± 0.66% fGFP-NSCs, 1.2% ± 0.58% fGFP-NSCs), and similar fractions were observed for the expression of myelinating mature oligodendrocyte marker myelin basic protein (MBP) in both fGFP-iNSCs and fGFP-NSCs (1.8% ± 0.62% and 1.8% ± 0.69%, respectively) (Figure 2B). We also found that 11% ± 0.97% of fGFP-iNSCs and 11% ± 2.1% of fGFP-NSCs expressed the helix-loop-helix transcription factor Olig2, a marker for oligodendroglial precursors (Figures 2A and 2B). The remaining proportion of cells stained for the multipotent stem cells marker SRY (sex-determining region Y)-box 2 (Sox2) (16% ± 2.3% fGFP-iNSCs and 17% ± 2.3% fGFP-NSCs) (Figures 2A and 2B) and nestin (6.4% ± 1.3% fGFP-iNSCs and 5.2% ± 1.0% fGFP-NSCs) (Figure 2B).

Histopathological analysis 7 weeks after transplantation revealed a significant reduction of the lesion volume in transplanted mice, both fGFP-NSC and fGFP-iNSC, compared to controls (Figure 2C). No significant differences were observed in the glial scar volume (GFAP-positive volume) surrounding the lesion epicenter in the transplant groups versus the control group (Figure 2D), nor was there any difference in the demyelination area between groups (Figure S2C).

Local inflammatory response was evaluated by quantification of F4/80-positive cells, a marker for mononuclear phagocytes, revealing a significant increase of inflammatory cells upon transplantation of either fGFP-iNSCs or fGFP-NSCs (Figure S2D). When distinguishing between F4/80-positive cells showing an M1-like (pro-inflammatory, induced nitric oxide synthase [iNOS]-expressing) polarization or M2-like (anti-inflammatory, cluster of differentiation 206 [CD206]-expressing) polarization, we observed a moderate reduction of the M1-like subset in both transplanted groups (Figure S2E), with a reciprocal increase in the M2-like subset (Figure S2F).

Stem cell transplantation has been shown to stimulate neuroprotection through the secretion of neurotrophic factors.[6] The quantification of NeuN-expressing mature neurons revealed that the transplantation of either fGFP-iNSCs or fGFP-NSCs was also able to significantly increase the number of surviving neurons in the ventral horns of the spared tissue surrounding the lesion area (Figure 2E). qPCR analysis revealed a substantial augmentation of the neurotrophin *brain-derived neurotrophic factor* (*Bdnf*) mRNA in tissue from transplanted groups (Figure S2G).

These data support the therapeutic potential of iNSC transplantation. Nevertheless, there remain some limitations in promoting tissue healing that we envisioned to overcome in this study with a combinatorial approach.

Acute and Chronic Overexpression of Lcn2 Is Observed in a Moderate Contusive Model of SCI

To identify the ideal window of opportunity for the injection of the anti-*Lcn2* 3WJ (3WJ-L12), we first characterized *Lcn2* expression in the injured spinal cord.

Protein expression analysis by western blot revealed a significant increase in Lcn2 expression at 1 dpi (Figure 3A). The same significant increase was also observed at the mRNA level, followed by a second

volumes measured as GFAP-positive volume at 56 dpi. Data are expressed % of GFAP-positive volume over the volume of selected spinal cord segment. Data represent minimum to maximum volume from n ≥ 5 mice per group. (E) Quantification of spared NeuN-positive neuronal cells in the ventral horns at 56 dpi. NeuN-positive cells were quantified using coronal serial sections of the lesioned area and perilesional area (±1,200 μm). Data are mean numbers per mm^2 (±SEM) from n = 5 mice per group. *$p < 0.05$ and **$p < 0.01$, versus PBS. Scale bars: 100 μm in (A); 1 mm in (C). Nuclei in (A) were stained with DAPI (blue). dpi, days post injury.

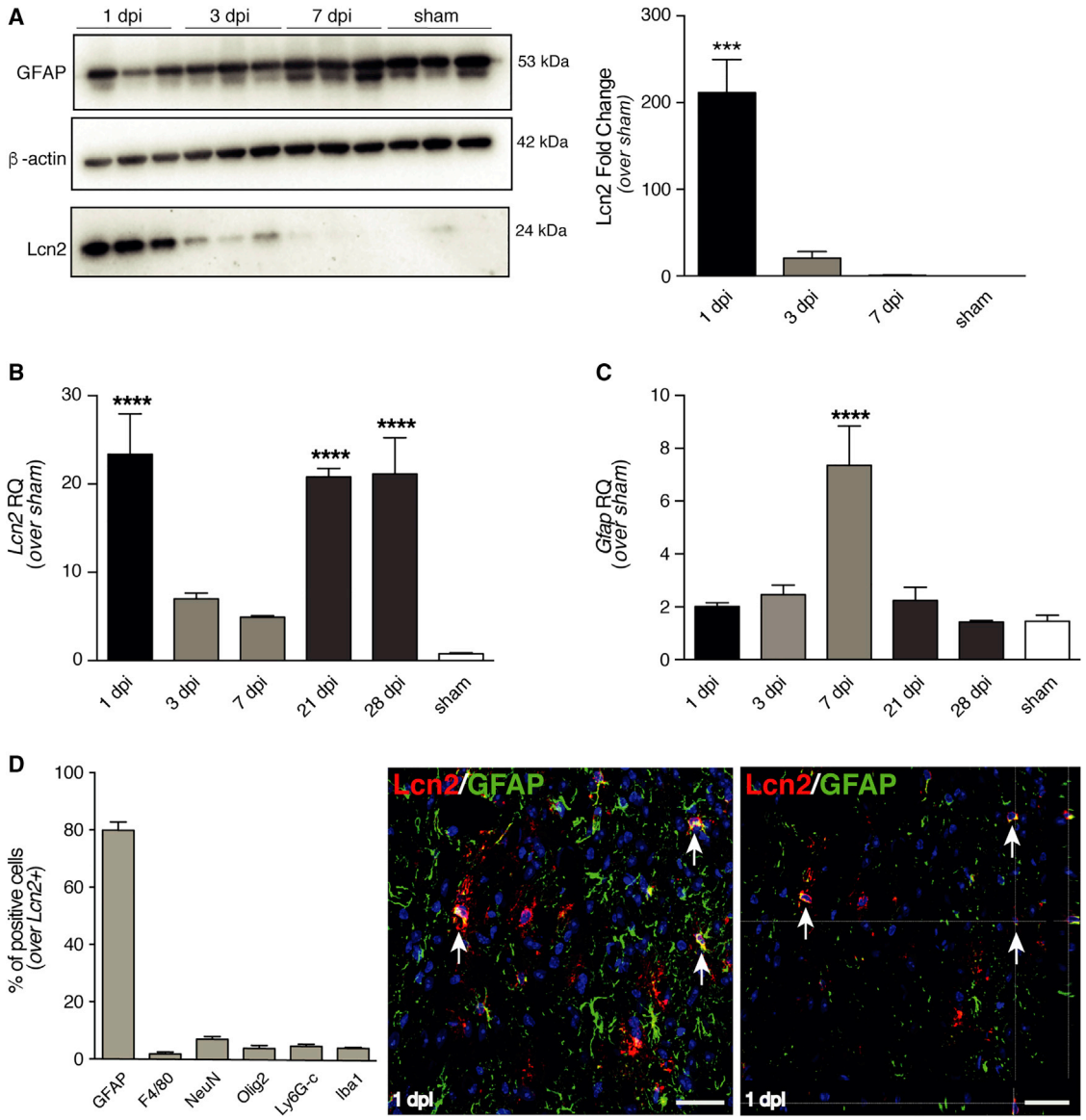

Figure 3. Expression of Lcn2 in Spinal Tissue upon Moderate Contusive SCI

(A) Representative western blot image of Lcn2 (24 kDa) and GFAP (53 kDa) expression, and densitometric quantification of n = 3 blots (right). β-actin (42 kDa) is used as loading control. Results are mean values relative to sham controls (±SEM). ***$p < 0.001$, versus sham. Control sham-treated mice (laminectomy only) were sacrificed 7 days post laminectomy. (B and C) qRT-PCR quantification of *Lcn2* (B) and *Gfap* (C) expression, reported as a relative quantification (RQ), versus *Gapdh*. Data are mean values (±SEM) from n = 3 mice. ****$p < 0.0001$, versus sham. Control sham-treated mice (laminectomy only) were sacrificed 7 and 28 days post laminectomy, and the average of the two time points has been used. (D) Relative percentages of cell types expressing Lcn2 in the spinal cord at 1 dpi. Data are expressed as mean % of double-positive cells over the total number of Lcn2-positive cells (±SEM) from n = 3 mice. Representative immunofluorescence micrographs of cells co-expressing Lcn2 and GFAP (arrows, right). Nuclei in D were stained with DAPI (blue). Scale bar, 20 μm. dpi, days post injury.

significant peak at 21 dpi and 28 dpi (Figure 3B). We also investigated the increase in *Gfap* mRNA levels upon SCI, revealing a significant increase in its expression in the subacute phase (7 dpi) (Figure 3C).

We then sought to characterize Lcn2-expressing cells at 1 dpi, revealing that the majority of Lcn2-positive cells co-stained for the astroglial marker GFAP in histopathological analyses (80% ± 3.0%) (Figure 3D). The remaining fraction of Lcn2-positive cells were similarly distributed among those co-expressing markers for mononuclear phagocytes (F4/80); neurons (NeuN); oligodendroglial cells (Olig2); monocytes, granulocytes, and neutrophils (common epitope on Ly-6G and Ly-6C lymphocyte antigen 6 complex locus G6D and locus C1); and microglia/macrophages (ionized calcium binding

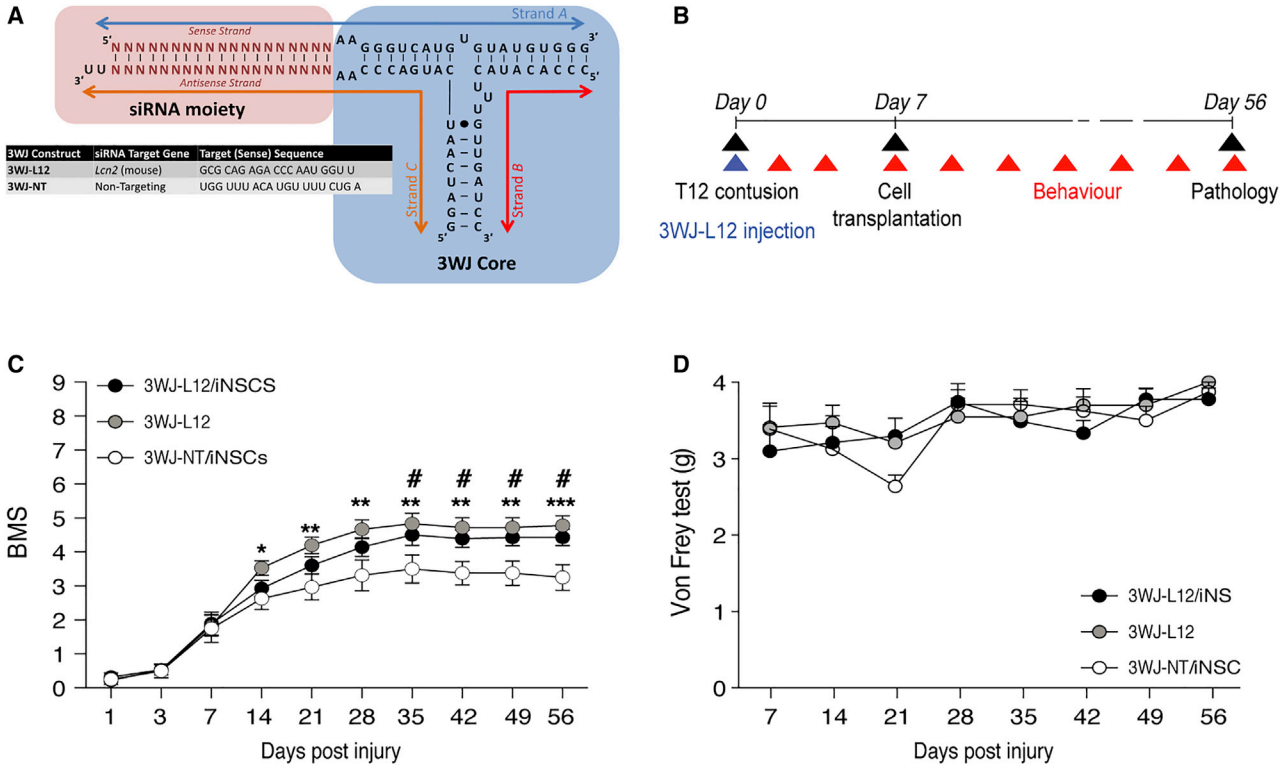

Figure 4. Combination of *In Situ* Acute 3WJ-*L12* and Subacute iNSC Transplantation Promotes Functional Recovery

(A) Generic 3WJ scheme depicting the three constituent RNA strands, variable siRNA and 3WJ core moieties (black circles indicate a wobble base pair). Target sequences of the variable siRNA moiety (N) are depicted for the anti-*Lcn2* (3WJ-L12) and the non-targeting 3WJ-NT. (B) Schematic representation of experimental design for acute injection of 3WJ-L12 into the lesion epicenter followed by subacute transplantation of fGFP-iNSCs. (C) Basso Mouse Scale (BMS) score evaluation of motor function recovery. Data are mean values (±SEM) from n ≥ 7 mice per group. *p < 0.05; **p < 0.01, and ***p < 0.001, 3WJ-L12-only versus 3WJ-NT/iNSCs. #p < 0.05, 3WJ-L12/iNSCs versus 3WJ-NT/iNSCs. (D) Assessment of mechanical allodynia by von Frey test. Data are mean values (±SEM) from n ≥7 mice per group. dpi, days post injury.

adaptor molecule 1, Iba1) (Figure 3D). At 21 dpi, the majority of Lcn2-positive cells were still found to express the astroglial marker GFAP (65% ± 1.2%), with the remaining fractions distributed among the above-mentioned markers (Figure S3).

Thus, based on these observations, we sought to target the acute (1 dpi) increase in Lcn2 expression via pRNA-RNAi, with the aim of generating a more amenable microenvironment for the subsequent transplantation of iNSCs and the ultimate goal of augmenting the therapeutic efficacy of iNSC grafts.

In Situ Acute 3WJ-*Lcn2* Administration and Subacute iNSC Transplantation Ameliorate Moderate Contusive Thoracic SCI in Mice

After assessing the therapeutic potential of the iNSC transplantation and having previously established the *in vivo* efficacy of 3WJ-Lcn2 to downregulate the target gene,[23] we aimed at combining the two approaches to achieve synergistic effects.

Thus, we pre-conditioned the lesion epicenter with 10 μg of the anti-*Lcn2* 3WJ named 3WJ-L12 (Figure 4A) immediately after delivery of a moderate contusive SCI; 1 week later we transplanted 150 × 10^3 iNSCs in four different sites surrounding the lesion area within the spinal cord parenchyma, approximately 500 μm distant from the lesion site (Figure 4B). As a control, we used mice treated with a combination of 10 μg of 3WJ-NT (an analogous pRNA-RNAi bearing a non-targeting siRNA moiety)[23] and sub-acutely transplanted with iNSCs. The effects of 3WJ-L12 were also evaluated in mice acutely injected with 3WJ-L12 only. By using the BMS score as an evaluation of gross locomotor functions, we observed a significant improvement in functional recovery in mice injected with 3WJ-L12, regardless of the transplantation of iNSC (Figure 4C). Mice treated with the 3WJ-L12 alone showed a significant improvement in locomotor capabilities from 14 dpi, whereas those receiving the combinatorial treatment (3WJ-L12 and iNSCs) did not show significant improvement until 35 dpi. Each of the three treatment groups was subject to the von Frey hair test, with no evidence of hindlimb allodynia (Figure 4D).

The 3WJ-L12-mediated modulation of *Lcn2* alone and as combinatorial therapy with iNSC transplantation instructed functional recovery in mice with moderate contusive SCI.

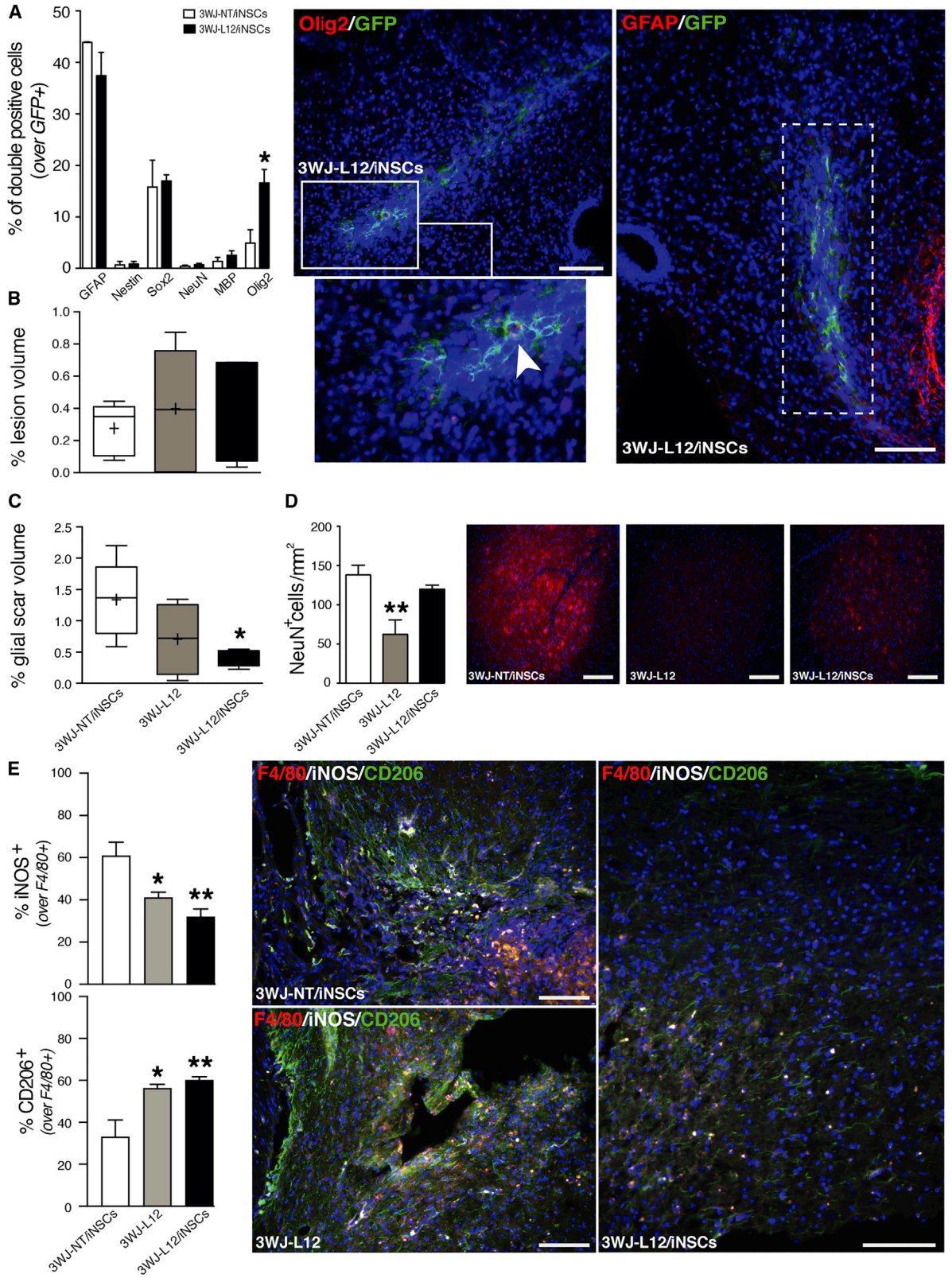

(legend on next page)

3WJ-L12 and iNSC Transplantation Combination Therapy Supports an Oligodendroglial Fate of Transplanted Cells and Ameliorates Secondary SCI Events

We first evaluated whether 3WJ-L12 injection affected the proportion of engrafted fGFP-iNSCs surviving in the host tissue. Immunohistochemical analysis revealed no difference in the percentage of surviving cells between the 3WJ-NT/iNSC control group and the 3WJ-L12/iNSC treatment (Figure S4A), nor were there any substantial difference in migration at 49 dpt (Figure S4B).

By identifying different cellular lineages using immunocytochemistry, we quantified the differentiation fate of surviving iNSCs. We observed that the majority of fGFP-iNSCs expressed GFAP (44% ± 0.14% in 3WJ-NT/iNSC, 37% ± 4.5% in 3WJ-L12/iNSC) (Figure 5A). However, we did observe a significant increase in the fraction of Olig2-positive grafted cells in the group treated with 3WJ-L12/iNSC (17% ± 2.6%) compared to the 3WJ-NT/iNSCs control group (5.0% ± 2.6%) (Figure 5A). The remaining fGFP-iNSCs expressed comparable means of the other cell lineage markers examined between groups: nestin (0.69% ± 0.69% 3WJ-NT/iNSC, 0.85% ± 0.57% 3WJ-L12/iNSC); Sox2 (16% ± 5.2% 3WJ-NT/iNSC, 17% ± 1.2% 3WJ-L12/iNSC); NeuN (0.55% ± 0.29% 3WJ-NT/iNSC, 0.52% ± 0.41% 3WJ-L12/iNSC); and MBP (1.4% ± 0.75% 3WJ-NT/iNSC, 2.6% ± 0.86% 3WJ-L12/iNSC) (Figure 5A).

To further assess the therapeutic effects of this combinatorial approach on secondary mechanisms upon moderate contusive SCI, we analyzed the lesion and the glial scar volumes surrounding the lesion epicenter. We observed no significant differences among groups with respect to lesion volume (Figure 5B), whereas a significant reduction of the glial scar was achieved with the 3WJ-L12/iNSC combination approach (Figure 5C).

We also evaluated neuronal survival by counting the number of NeuN-positive neurons within the ventral horns, observing a significant reduction in mice receiving the 3WJ-L12-only treatment (Figure 5D). The quantification of the demyelinated area did not show any difference between the three groups (Figure S4C), whereas the quantification of F4/80-positive cells within the injured spinal cord showed a small reduction in the 3WJ-L12-treated group (Figure S4D).

The analysis of the M1/M2 polarization of these F4/80-positive cells further revealed a significant decrease in the fraction of M1-like pro-inflammatory (iNOS/F4/80-positive) cells, accompanied by a significant increase in the fraction of M2-like anti-inflammatory (CD206/F4/80-positive) cells in both 3WJ-L12-treated groups (3WJ-L12 only and 3WJ-L12/iNSC) (Figure 5E), with the combinatorial treatment engendering the larger polarization dichotomy.

Therefore, the combination of pRNA and the here-validated stem cell therapeutics promoted the differentiation of transplanted iNSCs toward an oligodendroglial fate, modulated SCI secondary events such glial scarring, and promoted neuroprotection, tissue healing, and an anti-inflammatory response.

DISCUSSION

Traumatic SCIs are characterized by a cascade of molecular and cellular events, such as inflammation, continuous cell death, astrogliosis, and glial scarring,[28] that ultimately lead to different degrees of paralysis in correlation with the severity and location of the initial trauma.

Due to the complexity of these pathologies, it has become increasingly accepted that a combination of synergistic therapeutic approaches would be the optimal approach to treatment. In this study, we propose the combination of two innovative interventions: pRNA nanotechnology, herein aimed to modulate the expression of *Lcn2*, and the transplantation of murine-derived iNSCs.

Our data confirm three key findings: first, iNSC transplantation, as a highly translational approach, showed similar beneficial effects compared to bona fide NSCs, although both elicited rather limited functional regeneration in this moderate contusion SCI model. Second, downregulation of *Lcn2* yielded improvement of locomotor capabilities and reduced inflammatory responses, confirming its detrimental role in SCI. Third, the combination of our two iNSC treatments showed synergistic amelioration of secondary effects, not only highlighting the importance of such an approach but also paving the way for future studies using the technologies employed herein.

Figure 5. Combination of *In Situ* Acute 3WJ-L12 and Subacute iNSC Transplantation Ameliorates Secondary Damage and Promotes Oligodendroglial iNSC Differentiation

(A) Quantification of grafted fGFP-positive iNSCs co-expressing differentiation markers at 56 dpi. Data are mean % of double-positive cells over the total number of GFP-positive cells (±SEM) from n = 3 mice per group. *p < 0.05, versus 3WJ-NT/iNSCs. Representative immunofluorescence micrographs depicting engrafted GFP-positive iNSCs co-expressing astroglial marker GFAP (red) or immature oligodendroglial marker Olig2 (red) at 56 dpi (arrow). White rectangular area points to magnification snapshots. (B) Stereological quantification of lesion volumes expressed as % of lesion volume over the volume of selected spinal cord segment. Data represent minimum to maximum, n ≥ 5 mice per group. x axis as per (C) below. (C) Stereological quantification of glial scar volumes measured as GFAP-positive volume at 56 dpi. Data are expressed % of GFAP-positive volume over the volume of selected spinal cord segment. Data represent minimum to maximum volume, n ≥ 4 mice per group. *p < 0.05, versus 3WJ-NT/iNSCs. (D) Left: quantification of spared NeuN-positive cells in the ventral horns of experimental groups mice at 56 dpi. NeuN-positive cells were quantified using coronal serial sections of the lesioned area and perilesional area (±1,200 μm). Data are mean numbers per mm^2 (±SEM) from n = 5 mice per group. **p < 0.01, versus 3WJ-NT/iNSCs. Right: representative immunofluorescence micrographs depicting NeuN-positive cells. NeuN in red. (E) Number of iNOS-positive cells and number of CD206-positive cells over the total number of F4/80-positive cells at 56 dpi. Data are mean % of double-positive cells over the total number of F4/80-positive cells (±SEM) from n ≥ 3 mice per group. *p < 0.05 and **p < 0.01, versus 3WJ-NT/iNSCs. Right: representative immunofluorescence micrographs depicting F4/80-positive cells co-expressing iNOS or CD206. x axis of the top graph (iNOS) as per that of the graph below (CD206). Nuclei in (A), (D), and (E) were stained with DAPI (blue). Scale bars, 100 μm. dpi, days post injury.

In our study, we first aimed at characterizing the therapeutic effects of transplanted iNSCs by comparing them to the well-characterized NSCs in a model of moderate contusive thoracic SCI.[9,24,29] Our results showed that subacute iNSC transplantation promoted improvements of fine locomotor capabilities and modulation of major secondary events, like injury volume and neuroprotection, to a degree comparable to an NSC-transplanted group.

While cell transplantation in SCI research has shown promising results in pre-clinical studies, its translation into clinical application has so far been limited. We thus sought to augment the effects of iNSC transplantation by first modulating the detrimental nature of the injury site using pRNA-RNAi nanostructures to modulate Lcn2 expression.

Recent years have seen siRNA-based drugs reach the market,[30] and nanotechnology has greatly advanced the development of drug-delivery platforms.[31] Specific to the purposes of this study, bioinspired pRNA nanostructures are a promising example of this technology. Notably, our *in vivo* study represents one of the first applications of such nanotechnology in the CNS environment. Toward this goal, our group previously identified *Lcn2* as a potential target for pRNA-RNAi, demonstrating *in vitro* the efficacy of 3WJ-L12 in downregulating our target gene without invoking cytotoxicity and immunogenicity. Moreover, our group also provided preliminary *in vivo* data showing the capability to significantly downregulate *Lcn2* in a murine model of moderate contusive SCI by delivering 3WJ-L12 at a relatively low dose (10 μg).[23]

Lcn2 acts as a cytokine and plays a regulatory role in a broad range of inflammatory reactions.[15,32,33] It has been implicated as an autocrine mediator of reactive astrogliosis by several *in vitro* and *in vivo* studies, which demonstrated the protein's capability to sensitize astrocytes to cell death signals evident during CNS inflammation and has revealed the role of astrocyte-secreted Lcn2 as mediator of neurotoxicity during various disease states or neurodegenerative conditions.[17,34–36] Moreover, RNA sequencing (RNA-seq) data from spinal cord astrocytes has shown a significant increase in *Lcn2* expression upon injury.[37] Downregulation of Lcn2 in the injury environment might therefore alleviate inflammation and astroglial reactivity while promoting neuronal survival.

We observed an early spike in *Lcn2* expression upon moderate contusive injury (1 dpi), followed by a later, chronic induction. The goal of our study was to pre-condition the injured microenvironment in preparation for the transplantation of iNSCs; as such, we identified as our therapeutic target the acute *Lcn2* upregulation at 1 dpi. Future optimization of the intervention may benefit from identifying the ideal intervention window, perhaps by including a second or later treatment to address the chronic Lcn2 induction. At 1 dpi, the majority of cells expressing Lcn2 were astrocytes. Nevertheless, we also observed a small proportion of inflammatory cells expressing Lcn2, as previously described.[18]

Thus, in order to target a broad range of Lcn2-expressing cell sources, we did not functionalize our pRNA-RNAi therapeutics with any aptamer or other targeting moiety intended to address a specific cell population, opting instead for delivering it indiscriminately through lipofection. It is worth noting that in our previous *in vivo* evaluation of 3WJ-L12 delivery, no effect on Lcn2 downregulation was seen upon administration of the lipofection vehicle only (Lipofectamine RNAiMAX) or by the control non-targeting 3WJ-NT nanostructure. We compared our combinatorial therapy to the control group represented by the combination of 3WJ-NT with iNSC transplantation, while also taking into consideration a single injection of 3WJ-L12 in a separate group to investigate any effect derived from the RNA-only approach. We observed a significant improvement in locomotor capability from both 3WJ-L12 injection groups (with or without iNSCs), suggesting that acute downregulation of *Lcn2* results in the promotion of functional recovery, thus confirming Lcn2 as a potential therapeutic target for SCI.[18] Nonetheless, considering the limitation of our moderate contusive murine SCI in sufficiently impacting gross hindlimb functions[38] as detected with the BMS score, we aimed to investigate any putative synergistic effects through histopathological analysis.

The role of the glial scar within the SCI context has long been a subject of debate.[37,39–43] Given that reactive astrocytes exert timing- and context-dependent contradictory effects after CNS insults, it may prove worthwhile to look for new therapeutic targets that modulate these different activities in a controllable fashion. With our combined therapeutic approach, we observed a significant reduction of the glial scar during the chronic stage, thus paving the way for future investigations aimed at further characterizing the phenotype of astrocytes upon 3WJ-L12 delivery and elucidating their influence on the injured microenvironment.

We were then prompted to assess the fate of transplanted iNSCs with or without 3WJ-L12 pre-treatment. As compared to the non-treated spinal cord, iNSCs engrafted following 3WJ-L12 administration showed a small reduction in astroglial differentiation accompanied by a significant increase in Olig2 expression, although no differences in demyelination were observed between the three groups. Olig2 is a marker of oligodendrocyte progenitor cells (OPCs), and both the promotion of OPC differentiation and the transplantation of OPCs have been shown to play important roles in the context of SCI.[44] While differentiation into fully remyelinating oligodendrocytes has long been a goal for translational SCI therapeutic applications, a recent publication from Duncan et al.[45] reported that oligodendrocyte remyelination did not represent a crucial factor for hindlimb stepping locomotion. While that study, like our own, has some crucial limitations due to the SCI model used (moderate thoracic contusion injury), which only partially affects gross locomotion and thus might hinder findings,[46] it also raises questions about the role of remyelination in SCI and other potential beneficial effects exerted by OPCs. Therefore, while these questions remain open, it is also tempting for us to speculate that the lack in observed differences in demyelination between the experimental groups may be due to the timing of our analysis (7 weeks post-transplantation). A future long-term study would likely help in revealing any further differentiation of Olig2-fGFP-iNSCs in

our combinatorial approach into fully mature and remyelinating oligodendrocytes.

Notably, iNSCs, when transplanted in conjunction with 3WJ-L12 pre-treatment, retained their capability to promote neuroprotection, as implied by NeuN-positive cell quantification. Delivery of 3WJ-L12 alone showed a significant reduction compared to both iNSC groups, confirming that the promotion of neuronal survival is a function of the cellular therapy.

Finally, investigation of the inflammatory response revealed fewer F4/80-positive cells upon delivery of 3WJ-L12, most notably in the 3WJ-L12-only treatment but also in the 3WJ-L12/iNSC combination. When dissecting the phenotype of this innate immune response, we observed that both the sole 3WJ-L12 treatment and treatment in combination with iNSCs resulted in a significant increase in anti-inflammatory M2-like cells, mirrored by a significant reduction of pro-inflammatory M1-like mononuclear phagocytes.

In conclusion, our data thus suggest that, compared to single therapeutic approaches, a combination of treatments effectively augments the synergistic effects of the single treatments and will likely result in more effective and favorable outcomes. We have employed for the first time, to the best of our knowledge, a versatile pRNA-nanotechnology within the context of CNS disease, having previously been widely adopted for pre-clinical cancer studies.[47] pRNA-RNAi nanoparticle-mediated amelioration of acute *Lcn2* induction seemingly promoted an anti-inflammatory environment after SCI, reducing glial scarring and supporting the OPC-differentiation and neuroprotective properties of subacutely transplanted iNSCs.

MATERIALS AND METHODS

Contusion Model of SCI in Mice and Behavioral Assessment

All experimental procedures were performed in accordance with the Animals (Scientific Procedures) Act 1986 Amendment Regulations 2012 following ethical review by the University of Cambridge Animal Welfare and Ethical Review Body (AWERB). Animal work was covered by the PPL 700/8840 (S.P.). SCI was performed as previously described.[23] Briefly, a total of n = 96 adult (6- to 8-week-old) male C57BL/6 mice (Charles River) were deeply anesthetized with 2% isoflurane in oxygen (1.5 L/min), and a single-vertebra laminectomy was performed in order to expose the spinal cord at the T12 level. A moderate injury was performed by delivering a 70 kdyne force from an Infinite Horizon Impactor (Precision Systems and Instrumentation). Buprenorphine (Temgesic) was provided pre- and post-operatively; enrofloxacin (Baytril; Bayer) was provided pre-operatively and once daily to prevent infections for 7 days following surgeries. Bladders were manually expressed twice daily for a week and then once daily for the remaining duration of the experiment.

Hindlimb locomotor recovery was evaluated by the open-field BMS, a 10-point scale.[48] All the evaluations were performed in blind conditions by 2 observers. Locomotor activity was monitored for 4 min in an open field prior to the delivery of contusive injury and then once weekly for the remaining duration of the experiment. For statistical analysis of the BMS score, the mean of the left and right hindlimb scores was taken to yield a single BMS score per mouse. BMS subscore, assessed as previously described,[48] was performed only on mice with a BMS score greater than or equal to 5.

Sensory functions were assessed by von Frey test (Aesthesio) following the "up and down" method.[49] Briefly, mice were placed onto an elevated grid and left to acclimatize for 15 min prior to the test. Testing was initiated with the 1.4 g filament. A positive response was defined as withdrawal, or licking or shaking in the stimulated hind-paw within 3 s. This procedure was repeated until 3 positive or negative responses were achieved, for a maximum of 6 times, and 5 min was allowed between each session. In case of a positive response, the next weaker stimulus was presented; in case of a negative response, the next stronger stimulus was applied. The mice were tested prior to surgery to identify any sensory abnormalities (and thus withdraw the mouse from continued inclusion in the experiment), defined as sensitivity to the lowest force applicable (0.008 g; no mice were found with such abnormalities); mice were then tested once a week for the entire duration of the experiment. The Hargreaves apparatus (Ugo Basile) was employed to apply thermal pain stimulation in order to measure hyperalgesia to thermal stimulation in unrestrained animals.[50] Mice were placed onto a plexiglass surface and left to acclimatize for 15 min prior to testing. The Hargreaves' apparatus was set at 30% intensity and 20 s was established as a cutoff time to avoid tissue damage. Mice were again tested prior to surgery to identify any abnormalities (and thus withdraw the mouse from continued inclusion in the experiment), defined as a 20 s cutoff over the 3 repetitions in order to avoid any potential burn injury[51] (no mice were found with such abnormalities); mice were then tested once a week for 6 weeks after the injury. For each mouse, the heat source was applied to the plantar surface of the hindpaws until the animal withdrew from the noxious thermal stimulus, measuring the time of reaction. 5 min was allowed between each session. Measurements were repeated 3 times for each paw.

Synthesis of RNA Nanoparticles

pRNA-derived 3WJ nanoparticles bearing anti-Lcn2 (3WJ-L12) or non-targeting (3WJ-NT) siRNA moieties were designed and synthesized as previously described[23] using methods adapted from Shu et al.[52] Briefly, each 3WJ was assembled by annealing together equimolar amounts of its three constituent RNA strands (*A*, *B*, and *C*) in 1X tris/magnesium/saline (TMS) buffer. The RNA strands complemented each other in such a way as to readily assemble around the pRNA 3WJ core with an extended siRNA arm. The longer *A* and *C* strands, which contained the sense and antisense strands of the siRNA payloads, respectively, were transcribed from corresponding DNA templates using a Durascribe T7 transcription kit (Epicenter) and purified using native polyacrylamide gel electrophoresis (PAGE) and ethanol/sodium acetate precipitation. The shorter *B* strand, common to both 3WJs used in this study, was obtained from a commercial source. All RNA was 5′-dephosphorylated to avoid triggering retinoic acid-induced gene 1 (RIG-I)-mediated

Table 1. Primary and Secondary Antibody

Antibody	Supplier	Dilution
Mouse anti-NeuN	Millipore	1:250
Chicken anti-GFAP	Abcam	1:500
Rat anti-F4/80	Bio-Rad	1:250
Rabbit anti-Olig2	Millipore	1:500
Rabbit anti-Sox2	Abcam	1:100
Mouse anti-Nestin	Abcam	1:250
Rat anti-MBP	AbD Serotec	1:100
Rat anti-Ly6G-C	BD Biosciences	1:100
Rabbit anti-Iba1	Thermo Fisher	1:100
Mouse anti-iNOS	BD Biosciences	1:100
Rabbit anti-CD206	Abcam	1:400
Rat anti-Lcn2	R&D Systems	1:200
Chicken anti-GFP	Abcam	1:500
Rabbit anti-Ki67	Abcam	1:250
sAlexaFluor546 goat anti-mouse	Invitrogen	1:1,000
AlexaFluor647 goat anti-mouse	Invitrogen	1:1,000
AlexaFluor488 goat anti-chicken	Invitrogen	1:1,000
AlexaFluor546 goat anti-chicken	Invitrogen	1:1,000
AlexaFluor647 goat anti-chicken	Invitrogen	1:1,000
AlexaFluor546 goat anti-rat	Invitrogen	1:1,000
AlexaFluor647 goat anti-rat	Invitrogen	1:1,000
AlexaFluor488 goat anti-rabbit	Invitrogen	1:1,000
AlexaFluor546 goat anti-rabbit	Invitrogen	1:1,000
AlexaFluor647 goat anti-rabbit	Invitrogen	1:1,000

antiviral immunity and incorporated 2′-fluoro modified pyrimidines to afford greater nuclease resistance. Quantification of 3WJ nanostructures was by NanoDrop spectrophotometer (Thermo Fisher).

NSC Transplantation and Combinatorial Approach

Murine fGFP NSCs and iNSCs were prepared as previously described.[9] Seven days after injury (subacute phase) cells were resuspended in ice-cold 1× PBS at a concentration of 150×10^3 cells/μL and kept in ice prior to injection. Mice were anesthetized as mentioned above, and the laminectomy site was re-exposed. Fibrotic tissue was removed by using Dumont #4 forceps (Fine Science Tools), and with the help of a sterile needle a small hole was created in the dura mater in order to allow the entrance of the injecting needle. The volume to inject (250 nL/injection site) was withdrawn and injected with a pump under a surgery microscope by using a 5 μL Hamilton syringe with a short 33G needle placed onto a micromanipulator (World Precision Instruments). Each mouse received a total of four injections of either iNSCs (150×10^3 cells/μL), NSCs (150×10^3 cells/μL), or an equal volume of vehicle, administered bilaterally from midline at both the anterior aspect of T13 and the posterior aspect of T11. All cells used were at passage number $\leq$25. When a combinatorial approach was used, 10 μg of 2′F-modified 3WJ-L12 was delivered via transfection after performing moderate injury: 250 nL of the liposomal transfection agent Lipofectamine RNAiMAX (Life Technologies) was used to transfect a solution of the 3WJ into the parenchymal lesion center using a 5 μL syringe with a short 33G needle (Hamilton), with a total injection volume of 500 nL. Control animals received equivalent injection volumes of 10 μg of the negative control 2′F-modified-3WJ-NT.

Tissue Processing and *Ex Vivo* Pathology

Mice were anesthetized with an intra-peritoneal injection of ketamine 10 mg/mL (Boehringer Ingelheim) and xylazine 1.17 mg/mL (Bayer) and transcardially perfused with saline (sodium chloride 0.9%) plus 0.5 M ethylenediaminetetraacetate (EDTA; Sigma), followed by cold 4% paraformaldehyde (PFA) in PBS pH 7.4. The spinal cords were post-fixed in the same solution for 12 h at 4°C and then washed with 1× PBS. The dissected spinal cords were cryoprotected for at least 24 h in 30% sucrose (Sigma) in 1× PBS at 4°C, then the cords were embedded in Optimal Cutting Temperature (OCT) Compound (VWR Chemicals) and frozen using dry ice. Frozen cord blocks were placed in a cryostat (CM1850; Leica), and 30-μm-thick axial sections or 10-μm-thick sagittal sections were cut and collected onto SuperfrostPlus slides (ThermoScientific). A total of 10.5 mm of each cord segment, centered on the lesion site, was cut and collected onto slides resulting in either alternate serial sections with 30-μm-thick axial sections (600 μm apart) or 10 μm-thick sagittal sections (200 μm apart). Sections were then stored at −80°C until needed.

A total of n = 16 30-μm-thick sections per mouse were used for quantification of cell differentiation after transplantation, migration of grafted cells, Lcn2-expressing cells, or pro- or anti-inflammatory infiltrates. Mounted spinal cord sections onto coverslips were washed with 1× PBS before being incubated in blocking solution (1× PBS containing 0.1% Triton X-100 [Sigma] and 5% normal goat serum [NGS; Sigma]) for 60 min at room temperature. Sections were then incubated with the desired primary antibodies diluted in the blocking solution (Table 1) overnight at 4°C. Sections were then rinsed in 1× PBS, 0.3% Triton X-100 (Sigma), and incubated with the species-appropriate fluorochrome-conjugated secondary antibodies (1:1,000 dilution in blocking solution, Table1) for 60 min at room temperature. Coverslips were subsequently washed with 1× PBS before cell nuclei were counterstained with a 1 μg/mL solution of 4′,6-diamidino-2-phenylindole (DAPI; Roche) in 1× PBS for 5 min at room temperature. After a final wash, coverslips were mounted onto slides with fluorescence mounting medium (Dako). Quantifications were obtained from randomized spinal cords for each group, and images were acquired using a vertical epifluorescence microscope (Leica DM6000) or a confocal microscope (Leica TCS SP5 Microscope); n $\geq$ 100 cells for each marker have been quantified and images processed using the Fiji software package.[53] Data are expressed as a percentage of double-positive over the total number of $fGFP^+$ cells or $F4/80^+$ cells (mean ± SEM).

For neuronal survival quantification, a total of n = 5 30-μm-thick sections per mouse were used; tissue was processed as described above.

Briefly, after incubation with blocking solution, sections were then incubated with the anti-NeuN antibody (1:250, Millipore) in the blocking solution overnight at 4°C. Sections were then rinsed in 1× PBS, 0.1% or 0.3% Triton X-100 (Sigma) and incubated with the species-appropriate fluorochrome-conjugated secondary antibodies (1:1,000 dilution in blocking solution, Table 1) for 60 min at room temperature. Neuronal survival was then quantified by counting the number of NeuN-positive cells in the ventral horn. Images were acquired using a vertical epifluorescence microscope (Leica DM6000). Data are expressed as number of positive cells per mm^2 ± SEM.

For quantification of $GFAP^+$ volumes and lesion volumes, a total of n = 20 30-µm-thick sections per mouse or n = 8 10 µm sections per mouse were used, for graft survival a total of n = 16 30-µm-thick sections per mouse were used, and for inflammatory infiltrates a total of n = 18 30-µm-thick sections per mouse or n = 8 10-µm-thick sections per mouse were used. Tissue sections were pre-treated with peroxidase 3% for 15 min and then incubated for 1 h at room temperature in the blocking solution (1× PBS, 10% NGS [Sigma], 0.3% Triton X-100 [Sigma]). Anti-GFAP primary antibody (1:500, Abcam), or anti-GFP (1:200, Abcam), or anti-F4/80 (1:100, Biorad) were diluted in blocking solution (1× PBS, 1% NGS [Sigma], 0.3% Triton X-100 [Sigma]) and incubated at 4°C overnight. The following day, after washing the sections with 1× PBS, the appropriate biotinylated secondary antibody (biotinylated goat anti-chicken, 1:500 [Vector]; biotinylated goat anti-rat 1:500, [Sigma]) was diluted in a solution of PBS + 1% NGS (Sigma), 0.3% Triton X-100 (Sigma), and incubated for 1 h at room temperature. Sections were then incubated with "A" and "B" components of Vectastain Elite ABC kit (Vector Laboratories) for 1 h at room temperature, and finally the reaction was developed using 3,3′-diaminobenzidine (DAB) following the supplier's instructions. The reaction was blocked by washing the sections with distilled water, and sections were counterstained with hematoxylin. The sections were then dehydrated with increasing concentration of aqueous alcohol solutions (50%, 70%, and 100% ethanol), washed in xylene (Merck), and mounted with a synthetic Eukitt mounting medium (Sigma). Glial scar and lesion contours were outlined from equally spaced axial spinal cord sections using an Olympus BX53 microscope with motorized stage and Neurolucida software (11.07 64-bit, Microbrightfield).

For quantification of demyelination, a total of n = 16 30-µm-thick sections per mouse were used; spinal cord sections were stained for Luxol fast blue (LFB)/periodic-acid Schiff, as previously described.[25] After equilibration in 1× PBS, slides were passed serially through 50%, 70%, and 100% ethanol and stained in LFB (Sigma-Aldrich) staining solution (0.1% LFB in 96% ethanol with 0.5% acetic acid) overnight at 56°C. The following day, slides were rinsed in 96% ethanol and subsequently in distilled water, before being put in 0.1% lithium carbonate (Sigma-Aldrich) for 15 min. Samples were then left in 70% ethanol until gray matter could be distinguished under an optical microscope (Olympus), and the differentiation process was blocked by rinsing the slides in distilled water. The slides were finally dehydrated with an ethanol series (50%, 70%, and 100%) and cleared with xylene (Merck) before being mounted with Eukitt mounting medium. The LFB-negative areas of equally spaced axial spinal cord sections were outlined using an Olympus BX53 microscope with motorized stage and Neurolucida software. Data are expressed as the percentage of LFB-negative tissue per section (±SEM).

qRT-PCR

Ex vivo samples were collected at different time points following moderate contusion. RNA was extracted as per Smith et al.[23] Briefly, spinal cord segments were gently detached from 4–5 coverslips using a blade and placed into a 1.5 mL tube. Total RNA was then extracted by resuspending tissues in 500 mL of TRI Reagent (Sigma) and incubating at room temperature for 10 min. Proteinase K from Tritirachium album (Sigma) was activated at 37°C for 10 min prior to addition to the TRI/RNA solutions at a 1:100 dilution and incubated at 55°C for 2 h, followed by 80°C for 15 min. RNA was then isolated, reverse transcribed, and subjected to qPCR as below.

TRI/RNA solutions were mixed with 20% vol chloroform (Sigma), incubated for 2–3 min and spun at 12,000 × *g* for 15 min at 4°C. The upper aqueous phase was collected into a new 1.5 mL tube and added to an equal volume of 2-propanol (Sigma). The solutions were then incubated at room temperature for 10 min and spun at 12.000 × *g* for 30 min at 4°C. Pellets were washed twice with 600 µL of 70% ethanol, spun at 12.000 × *g* for 15 min and left to air-dry under a fume hood. Pellets were then resuspended in 10 µL nuclease-free water (Invitrogen) and heated at 55°C for 10 min at 300 rpm in a thermomixer (Eppendorf). RNA was then quantified using a NanoDrop 2000 spectrophotometer (Thermo Fisher Scientific). 500 ng of total RNA was used for cDNA transcription using a High-Capacity cDNA Reverse Transcription kit (Life Technologies) using random hexamer primers. qRT-PCR was subsequently performed using TaqMan reagents (TaqMan Fast Universal PCR Master Mix and 6-carboxyfluorescein (FAM)-labeled *Bdnf* TaqMan Gene Expression Assays, Mm01334047_m1) and an Applied Biosystems 7500 Fast real-time PCR system. Mouse *Gapdh* (VIC-labeled; 4352339E Life Technologies) was used as a reference gene for determining relative gene expression (relative quantification [RQ]) using the $2^{-\Delta\Delta Ct}$ method.[54] Each biological sample was measured in triplicate.

Western Blots

Proteins from PFA-fixed tissues were extracted by following a previously published protocol[55] and by first gently detaching spinal cord segments from 4–5 coverslips using a blade and placed into a 1.5 mL microfuge tube. Total protein was then extracted by resuspending the tissue in radioimmunoprecipitation assay (RIPA) buffer (10 mM Tris HCl, 0.1 M, pH 7.2; 1% sodium deoxycholate; 1% Triton X-100; 3% sodium dodecyl sulfate [SDS]; 150 mM NaCl, 1.5 M; 1 mM EDTA, pH 8.0, 0.5 M [Thermo Fisher Scientific]; 1 mM phenylmethanesulfonyl fluoride [Sigma]; Complete Protease Inhibitor cocktail [Roche]; Halt Phosphatase Inhibitor [Thermo Fisher Scientific]) for 20 min at 100°C. Samples were then placed on ice for 20 min, followed by sonication (Bioruptor Plus sonication device; Diagenode Innovating Epigenetics Solutions). Samples were then spun, and

supernatants were collected for protein quantification. Protein quantification was performed using a Pierce BCA Protein Assay kit (Thermo Scientific). 30 μg of total protein were mixed with NuPAGE LDS Sample Buffer (Life Technologies), NuPAGE Sample Reducing Agent (Life Technologies), and distilled water prior to being heated at 95°C for 5 min. Proteins were separated by SDS-PAGE in a 4%–12% Bis-Tris gel using a Novex Bolt Mini Gel system and running buffer (Tris 25 mM, glycine 192 mM, SDS 10%) before being transferred onto Immobilon-P polyvinylidene fluoride membranes (0.45 mm pore size; Millipore) in transfer buffer (Tris 25 mM, glycine 192 mM, methanol 20%) for 1 h 45 min at 4°C using a Novex Bolt Mini Blot Module. A SeeBlue Plus2 standard (Life Technologies) was used to estimate protein sizes, and transfer was confirmed by Ponceau S (Sigma) staining. Immunoblot was obtained by first blocking membranes for 1 h at room temperature with a solution of 0.1% Tween 20 and 5% dried skimmed milk powder (Marvel) in 1× PBS (pH 7.4) and then incubated with primary antibodies overnight at 4°C (rat anti-Lcn2, 1:1,000 [R&D System]; rabbit anti-GFAP, 1:10,000 [Dako]; mouse anti-β-actin, 1:10,000 [Sigma]) diluted in antibody solution (0.1% Tween 20, 5% dried skimmed milk powder in 1× PBS). After washing with 1× PBS Containing 0.1% Tween 20, the membranes were incubated with the species-appropriate horseradish peroxidase-conjugated secondary antibodies (Thermo Scientific) for 1 h at room temperature at a 1:10,000 dilution in blocking solution. Immunoreactivity was revealed using Western Lightning Plus-ECL (PerkinElmer) and imaged using a Bio-Rad Chemi-Doc XRS+ system with Image Lab 5.1 software (Bio-Rad). Densitometry measurements were performed using Fiji, with each protein band being normalized to the β-actin loading controls.

Statistical Analysis

Statistical analyses were performed using the GraphPad Prism 6 software package. One-way analysis of variance (ANOVA) followed by Dunnett's multiple comparison test was used for comparison of three or more experimental groups, whereas two-way repeated-measures ANOVA with Bonferroni post-tests was used for multi-group comparisons under multiple conditions. Graphical results are expressed as the mean ± SEM. Statistical analysis was conducted at 95% confidence level. A p value less than 0.05 was considered as statistically significant (*$p < 0.05$; **$p < 0.01$; ***$p < 0.001$; or ****$p < 0.0001$, versus controls). Specifics of the number of biological replicates of each experiment are detailed in the corresponding figure captions.

SUPPLEMENTAL INFORMATION

Supplemental Information can be found online at https://doi.org/10.1016/j.ymthe.2020.08.001.

AUTHOR CONTRIBUTIONS

Conceptualization: A.B., J.A.S., and S.P.; Methodology: A.B., J.A.S., and S.P.; Investigation, Validation, and Formal Analysis: A.B., J.A.S., S.B., R.H., and C.R.; Writing – Original Editing: A.B.; Writing – Review & Editing: A.B., F.E., J.A.S., and S.P.; Supervision: S.P.; Funding Acquisition: S.P.

CONFLICTS OF INTEREST

S.P. is co-founder, CSO, and shareholder (>5%) of CITC and iSTEM Therapeutics, and co-founder and Non-executive Director at asitia Therapeutics. J.A.S. is a Project Manager and Senior Research Associate at CITC and CSO of asitia Therapeutics.

ACKNOWLEDGMENTS

The authors wish to acknowledge Peixuan Guo, Luca Peruzzotti-Jametti, and Giovanni Pluchino for their technical contributions and critical insights throughout the execution of the study. The authors also thank Nunzio Vicario for his technical help. This work was funded by the European Research Council (ERC) under the ERC-2010-StG grant agreement No. 260511-SEM_SEM, the Bascule Charitable Trust (RG 75149 and RG 98181 to S.P.), the International Foundation for Research in Paraplegia (RG 69318 to S.P.), and Wings for Life (RG 82921 to S.P.).

REFERENCES

1. Jazayeri, S.B., Beygi, S., Shokraneh, F., Hagen, E.M., and Rahimi-Movaghar, V. (2015). Incidence of traumatic spinal cord injury worldwide: a systematic review. Eur. Spine J. *24*, 905–918.
2. Norenberg, M.D., Smith, J., and Marcillo, A. (2004). The pathology of human spinal cord injury: defining the problems. J. Neurotrauma *21*, 429–440.
3. Ahuja, C.S., Nori, S., Tetreault, L., Wilson, J., Kwon, B., Harrop, J., Choi, D., and Fehlings, M.G. (2017). Traumatic Spinal Cord Injury-Repair and Regeneration. Neurosurgery *80* (3S), S9–S22.
4. Silva, N.A., Sousa, N., Reis, R.L., and Salgado, A.J. (2014). From basics to clinical: a comprehensive review on spinal cord injury. Prog. Neurobiol. *114*, 25–57.
5. Griffin, J.M., and Bradke, F. (2020). Therapeutic repair for spinal cord injury: combinatory approaches to address a multifaceted problem. EMBO Mol. Med. *12*, e11505.
6. Giusto, E., Donegà, M., Cossetti, C., and Pluchino, S. (2014). Neuro-immune interactions of neural stem cell transplants: from animal disease models to human trials. Exp. Neurol. *260*, 19–32.
7. Martino, G., and Pluchino, S. (2006). The therapeutic potential of neural stem cells. Nat. Rev. Neurosci. *7*, 395–406.
8. Willis, C.M., Nicaise, A.M., Peruzzotti-Jametti, L., and Pluchino, S. (2020). The neural stem cell secretome and its role in brain repair. Brain Res. *1729*, 146615.
9. Peruzzotti-Jametti, L., Bernstock, J.D., Vicario, N., Costa, A.S.H., Kwok, C.K., Leonardi, T., Booty, L.M., Bicci, I., Balzarotti, B., Volpe, G., et al. (2018). Macrophage-Derived Extracellular Succinate Licenses Neural Stem Cells to Suppress Chronic Neuroinflammation. Cell Stem Cell *22*, 355–368.e13.
10. Shi, Y., Inoue, H., Wu, J.C., and Yamanaka, S. (2017). Induced pluripotent stem cell technology: a decade of progress. Nat. Rev. Drug Discov. *16*, 115–130.
11. Thier, M., Wörsdörfer, P., Lakes, Y.B., Gorris, R., Herms, S., Opitz, T., Seiferling, D., Quandel, T., Hoffmann, P., Nöthen, M.M., et al. (2012). Direct conversion of fibroblasts into stably expandable neural stem cells. Cell Stem Cell *10*, 473–479.
12. Thier, M.C., Hommerding, O., Panten, J., Pinna, R., García-González, D., Berger, T., Wörsdörfer, P., Assenov, Y., Scognamiglio, R., Przybylla, A., et al. (2019). Identification of Embryonic Neural Plate Border Stem Cells and Their Generation by Direct Reprogramming from Adult Human Blood Cells. Cell Stem Cell *24*, 166–182.e13.
13. Erharter, A., Rizzi, S., Mertens, J., and Edenhofer, F. (2019). Take the shortcut - direct conversion of somatic cells into induced neural stem cells and their biomedical applications. FEBS Lett. *593*, 3353–3369.
14. Ferreira, A.C., Dá Mesquita, S., Sousa, J.C., Correia-Neves, M., Sousa, N., Palha, J.A., and Marques, F. (2015). From the periphery to the brain: Lipocalin-2, a friend or foe? Prog. Neurobiol. *131*, 120–136.
15. Berard, J.L., Zarruk, J.G., Arbour, N., Prat, A., Yong, V.W., Jacques, F.H., Akira, S., and David, S. (2012). Lipocalin 2 is a novel immune mediator of experimental

autoimmune encephalomyelitis pathogenesis and is modulated in multiple sclerosis. Glia *60*, 1145–1159.

16. Marques, F., Mesquita, S.D., Sousa, J.C., Coppola, G., Gao, F., Geschwind, D.H., Columba-Cabezas, S., Aloisi, F., Degn, M., Cerqueira, J.J., et al. (2012). Lipocalin 2 is present in the EAE brain and is modulated by natalizumab. Front. Cell. Neurosci. *6*, 33.
17. Zamanian, J.L., Xu, L., Foo, L.C., Nouri, N., Zhou, L., Giffard, R.G., and Barres, B.A. (2012). Genomic analysis of reactive astrogliosis. J. Neurosci. *32*, 6391–6410.
18. Rathore, K.I., Berard, J.L., Redensek, A., Chierzi, S., Lopez-Vales, R., Santos, M., Akira, S., and David, S. (2011). Lipocalin 2 plays an immunomodulatory role and has detrimental effects after spinal cord injury. J. Neurosci. *31*, 13412–13419.
19. Guo, P. (2010). The emerging field of RNA nanotechnology. Nat. Nanotechnol. *5*, 833–842.
20. Guo, P., Zhang, C., Chen, C., Garver, K., and Trottier, M. (1998). Inter-RNA interaction of phage phi29 pRNA to form a hexameric complex for viral DNA transportation. Mol. Cell *2*, 149–155.
21. Shu, D., Li, H., Shu, Y., Xiong, G., Carson, W.E., 3rd, Haque, F., Xu, R., and Guo, P. (2015). Systemic Delivery of Anti-miRNA for Suppression of Triple Negative Breast Cancer Utilizing RNA Nanotechnology. ACS Nano *9*, 9731–9740.
22. Lee, T.J., Yoo, J.Y., Shu, D., Li, H., Zhang, J., Yu, J.G., Jaime-Ramirez, A.C., Acunzo, M., Romano, G., Cui, R., et al. (2017). RNA Nanoparticle-Based Targeted Therapy for Glioblastoma through Inhibition of Oncogenic miR-21. Mol. Ther. *25*, 1544–1555.
23. Smith, J.A., Braga, A., Verheyen, J., Basilico, S., Bandiera, S., Alfaro-Cervello, C., Peruzzotti-Jametti, L., Shu, D., Haque, F., Guo, P., and Pluchino, S. (2018). RNA Nanotherapeutics for the Amelioration of Astroglial Reactivity. Mol. Ther. Nucleic Acids *10*, 103–121.
24. Cusimano, M., Biziato, D., Brambilla, E., Donegà, M., Alfaro-Cervello, C., Snider, S., Salani, G., Pucci, F., Comi, G., Garcia-Verdugo, J.M., et al. (2012). Transplanted neural stem/precursor cells instruct phagocytes and reduce secondary tissue damage in the injured spinal cord. Brain *135*, 447–460.
25. Pluchino, S., Quattrini, A., Brambilla, E., Gritti, A., Salani, G., Dina, G., Galli, R., Del Carro, U., Amadio, S., Bergami, A., et al. (2003). Injection of adult neurospheres induces recovery in a chronic model of multiple sclerosis. Nature *422*, 688–694.
26. Kakuta, Y., Adachi, A., Yokohama, M., Horii, T., Mieda, T., Iizuka, Y., Takagishi, K., Chikuda, H., Iizuka, H., and Nakamura, K. (2019). Spontaneous functional full recovery from motor and sensory deficits in adult mice after mild spinal cord injury. Heliyon *5*, e01847.
27. Macias, M.Y., Syring, M.B., Pizzi, M.A., Crowe, M.J., Alexanian, A.R., and Kurpad, S.N. (2006). Pain with no gain: allodynia following neural stem cell transplantation in spinal cord injury. Exp. Neurol. *201*, 335–348.
28. Profyris, C., Cheema, S.S., Zang, D., Azari, M.F., Boyle, K., and Petratos, S. (2004). Degenerative and regenerative mechanisms governing spinal cord injury. Neurobiol. Dis. *15*, 415–436.
29. Pluchino, S., Zanotti, L., Rossi, B., Brambilla, E., Ottoboni, L., Salani, G., Martinello, M., Cattalini, A., Bergami, A., Furlan, R., et al. (2005). Neurosphere-derived multipotent precursors promote neuroprotection by an immunomodulatory mechanism. Nature *436*, 266–271.
30. Setten, R.L., Rossi, J.J., and Han, S.P. (2019). The current state and future directions of RNAi-based therapeutics. Nat. Rev. Drug Discov. *18*, 421–446.
31. Guo, S., Xu, C., Yin, H., Hill, J., Pi, F., and Guo, P. (2020). Tuning the size, shape and structure of RNA nanoparticles for favorable cancer targeting and immunostimulation. Wiley Interdiscip. Rev. Nanomed. Nanobiotechnol. *12*, e1582.
32. Jha, M.K., Jeon, S., Jin, M., Ock, J., Kim, J.H., Lee, W.H., and Suk, K. (2014). The pivotal role played by lipocalin-2 in chronic inflammatory pain. Exp. Neurol. *254*, 41–53.
33. Lee, S., Lee, J., Kim, S., Park, J.Y., Lee, W.H., Mori, K., Kim, S.H., Kim, I.K., and Suk, K. (2007). A dual role of lipocalin 2 in the apoptosis and deramification of activated microglia. J. Immunol. *179*, 3231–3241.
34. Lee, S., Park, J.Y., Lee, W.H., Kim, H., Park, H.C., Mori, K., and Suk, K. (2009). Lipocalin-2 is an autocrine mediator of reactive astrocytosis. J. Neurosci. *29*, 234–249.
35. Jin, M., Jang, E., and Suk, K. (2014). Lipocalin-2 Acts as a Neuroinflammatogen in Lipopolysaccharide-injected Mice. Exp. Neurobiol. *23*, 155–162.
36. Bi, F., Huang, C., Tong, J., Qiu, G., Huang, B., Wu, Q., Li, F., Xu, Z., Bowser, R., Xia, X.G., and Zhou, H. (2013). Reactive astrocytes secrete lcn2 to promote neuron death. Proc. Natl. Acad. Sci. USA *110*, 4069–4074.
37. Anderson, M.A., Burda, J.E., Ren, Y., Ao, Y., O'Shea, T.M., Kawaguchi, R., Coppola, G., Khakh, B.S., Deming, T.J., and Sofroniew, M.V. (2016). Astrocyte scar formation aids central nervous system axon regeneration. Nature *532*, 195–200.
38. Schucht, P., Raineteau, O., Schwab, M.E., and Fouad, K. (2002). Anatomical correlates of locomotor recovery following dorsal and ventral lesions of the rat spinal cord. Exp. Neurol. *176*, 143–153.
39. Faulkner, J.R., Herrmann, J.E., Woo, M.J., Tansey, K.E., Doan, N.B., and Sofroniew, M.V. (2004). Reactive astrocytes protect tissue and preserve function after spinal cord injury. J. Neurosci. *24*, 2143–2155.
40. Okada, S., Nakamura, M., Katoh, H., Miyao, T., Shimazaki, T., Ishii, K., Yamane, J., Yoshimura, A., Iwamoto, Y., Toyama, Y., and Okano, H. (2006). Conditional ablation of Stat3 or Socs3 discloses a dual role for reactive astrocytes after spinal cord injury. Nat. Med. *12*, 829–834.
41. Fawcett, J.W. (2006). Overcoming inhibition in the damaged spinal cord. J. Neurotrauma *23*, 371–383.
42. Pekny, M., and Nilsson, M. (2005). Astrocyte activation and reactive gliosis. Glia *50*, 427–434.
43. Swanson, R.A., Ying, W., and Kauppinen, T.M. (2004). Astrocyte influences on ischemic neuronal death. Curr. Mol. Med. *4*, 193–205.
44. Li, N., and Leung, G.K. (2015). Oligodendrocyte Precursor Cells in Spinal Cord Injury: A Review and Update. BioMed Res. Int. *2015*, 235195.
45. Duncan, G.J., Manesh, S.B., Hilton, B.J., Assinck, P., Liu, J., Moulson, A., Plemel, J.R., and Tetzlaff, W. (2018). Locomotor recovery following contusive spinal cord injury does not require oligodendrocyte remyelination. Nat. Commun. *9*, 3066.
46. Pukos, N., Goodus, M.T., Sahinkaya, F.R., and McTigue, D.M. (2019). Myelin status and oligodendrocyte lineage cells over time after spinal cord injury: What do we know and what still needs to be unwrapped? Glia *67*, 2178–2202.
47. Xu, C., Haque, F., Jasinski, D.L., Binzel, D.W., Shu, D., and Guo, P. (2018). Favorable biodistribution, specific targeting and conditional endosomal escape of RNA nanoparticles in cancer therapy. Cancer Lett. *414*, 57–70.
48. Basso, D.M., Fisher, L.C., Anderson, A.J., Jakeman, L.B., McTigue, D.M., and Popovich, P.G. (2006). Basso Mouse Scale for locomotion detects differences in recovery after spinal cord injury in five common mouse strains. J. Neurotrauma *23*, 635–659.
49. Chaplan, S.R., Bach, F.W., Pogrel, J.W., Chung, J.M., and Yaksh, T.L. (1994). Quantitative assessment of tactile allodynia in the rat paw. J. Neurosci. Methods *53*, 55–63.
50. Hargreaves, K., Dubner, R., Brown, F., Flores, C., and Joris, J. (1988). A new and sensitive method for measuring thermal nociception in cutaneous hyperalgesia. Pain *32*, 77–88.
51. Cheah, M., Fawcett, J.W., and Andrews, M.R. (2017). Assessment of Thermal Pain Sensation in Rats and Mice Using the Hargreaves Test. Bio Protoc. *7*, e2506.
52. Shu, Y., Shu, D., Haque, F., and Guo, P. (2013). Fabrication of pRNA nanoparticles to deliver therapeutic RNAs and bioactive compounds into tumor cells. Nat. Protoc. *8*, 1635–1659.
53. Schindelin, J., Arganda-Carreras, I., Frise, E., Kaynig, V., Longair, M., Pietzsch, T., Preibisch, S., Rueden, C., Saalfeld, S., Schmid, B., et al. (2012). Fiji: an open-source platform for biological-image analysis. Nat. Methods *9*, 676–682.
54. Livak, K.J., and Schmittgen, T.D. (2001). Analysis of relative gene expression data using real-time quantitative PCR and the 2(-Delta Delta C(T)) Method. Methods *25*, 402–408.
55. Guo, H., Liu, W., Ju, Z., Tamboli, P., Jonasch, E., Mills, G.B., Lu, Y., Hennessy, B.T., and Tsavachidou, D. (2012). An efficient procedure for protein extraction from formalin-fixed, paraffin-embedded tissues for reverse phase protein arrays. Proteome Sci. *10*, 56.